PCCP

RSC Publishing

PAPER

View Article Online
View Journal | View Issue

OH-initiated oxidation of sub-micron unsaturated fatty acid particles†

Cite this: *Phys. Chem. Chem. Phys.*, 2013, **15**, 18649

Theodora Nah,[ab] Sean H. Kessler,[c] Kelly E. Daumit,[d] Jesse H. Kroll,[cd] Stephen R. Leone[abe] and Kevin R. Wilson*[b]

Received 25th June 2013,
Accepted 18th September 2013

DOI: 10.1039/c3cp52655k

www.rsc.org/pccp

The heterogeneous reaction of OH radicals with sub-micron unsaturated fatty acid particles in the presence of H_2O_2 and O_2 is studied to explore how surface OH addition reactions initiate chain reactions that rapidly transform the chemical composition of an organic particle. In the presence of 20.7 ppm [H_2O_2] in a 10% mixture of O_2 in N_2, the effective uptake coefficients of oleic acid, linoleic acid and linolenic acid are found to be 1.72 ± 0.08, 3.75 ± 0.18 and 5.73 ± 0.14, respectively. These effective uptake coefficients are larger than unity, providing clear evidence for particle-phase secondary chain chemistry. The effective uptake coefficient increases linearly with the number of C=C double bonds in the unsaturated fatty acid molecule. Elemental composition analysis reveals that there is an addition of, on average, 0.57 ± 0.02, 0.61 ± 0.01 and 0.73 ± 0.04 O atoms per reactive loss of oleic acid, linoleic acid and linolenic acid, respectively, which suggests that OH addition to the C=C double bond is not the sole reaction pathway that consumes the molecular species. These results suggest the potential presence of secondary reactions that consume the unsaturated fatty acid molecular species without increasing the particulate oxygen content. As the unsaturated fatty acid particles become more oxygenated, volatilization also becomes significant. The magnitudes of the effective uptake coefficients are found to be dependent on the concentrations of OH, O_2 and H_2O_2 in the flow reactor. A plausible reaction mechanism is presented to show how surface OH addition reactions initiate chain reactions that rapidly transform an unsaturated organic particle's physicochemical properties.

1. Introduction

Free radical-initiated oxidation of hydrocarbons plays a key role in many important processes such as material synthesis, combustion, atmospheric chemistry, soot formation and oxidation. Given the importance of hydroxyl (OH) radicals in atmospheric and combustion chemistry, the reaction mechanisms and rates of OH radicals with a variety of gas phase hydrocarbons have been studied extensively.[1–3] Two classes of OH-initiated reaction mechanisms that are generally well-understood are hydrogen atom (H) abstraction and OH addition reactions, shown in eqn (1) and (2), respectively.

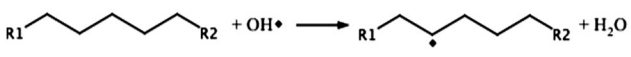

(1)

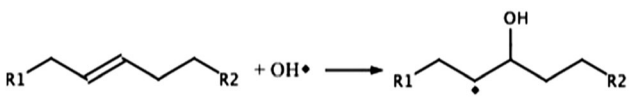

(2)

For the OH oxidation of saturated hydrocarbons, the reaction is initiated solely by the abstraction of a H atom by the OH radical to form an alkyl radical and H_2O (eqn (1)). In the case of unsaturated hydrocarbons, the reaction occurs either by H abstraction to form an alkyl radical and H_2O (eqn (1)) or by the addition of OH to the C=C double bond to form a hydroxyalkyl intermediate (eqn (2)). OH addition to the C=C double bond is found to be the dominant reaction channel for gas phase unsaturated hydrocarbons.[1–3] The rate coefficients for the OH oxidation of unsaturated hydrocarbons are also significantly faster than the OH oxidation of saturated hydrocarbons.[1–3] The alkyl and hydroxyalkyl radicals can react with O_2 to form peroxy and hydroxyperoxy radicals, respectively.[1–6] One important reaction pathway for the peroxy and hydroxyperoxy

[a] *Department of Chemistry, University of California, Berkeley, CA 94720, USA*
[b] *Chemical Sciences Division, Lawrence Berkeley National Laboratory, Berkeley, CA 94720, USA. E-mail: krwilson@lbl.gov*
[c] *Department of Chemical Engineering, Massachusetts Institute of Technology, Massachusetts 02139, USA*
[d] *Department of Civil and Environmental Engineering, Massachusetts Institute of Technology, Massachusetts 02139, USA*
[e] *Department of Physics, University of California, Berkeley, CA 94720, USA*

† Electronic supplementary information (ESI) available. See DOI: 10.1039/c3cp52655k

radicals is the peroxy radical + peroxy radical reaction[1–3] and the hydroxyperoxy radical + hydroxyperoxy radical reaction,[4–6] respectively. The peroxy radical self reaction produces higher molecular weight products with one oxygenated functional group,[1–3] while the hydroxyperoxy radical self reaction forms higher molecular weight products with two oxygenated functional groups.[4–6]

Recently, there has been an increased focus on the heterogeneous reaction of gas phase OH radicals with sub-micron organic particles due to the importance of particles in many environmental and combustion processes. The gas–particle interface is chemically distinct from the homogeneous environment of a gas or condensed phase. While reaction rates and product distributions depend upon the molecular structure and transition states in gas phase reactions, interfacial molecular orientation and thermodynamic phase may control reaction rates and product distributions for heterogeneous reactions. As a result, predictions of particle surface reactivity based solely on the molecular structure (*e.g.* the number and type of reactive sites in an isolated molecule) are often inaccurate.[7,8]

A key quantity for the reaction of OH radicals with sub-micron organic particles is the reaction probability or the reactive uptake coefficient, defined as the fraction of gas–particle collisions that results in a reaction. Obtaining a reactive uptake coefficient by measuring the reactive loss of gas phase radicals necessitates the reactive uptake coefficient to be less than or equal to 1. Alternatively, the heterogeneous reaction can be monitored *via* the loss of the particle phase molecular species to obtain an effective uptake coefficient. An effective uptake coefficient that is larger than unity indicates that more than one particle phase molecular species is lost for every gas–particle collision and is clear evidence for particle-phase secondary chemistry. Many groups studying the OH-initiated oxidation of organic particles have observed particle-phase secondary chemistry in this manner.[9–11]

To better understand fundamental OH-particle reaction mechanisms and kinetics, several studies have focused on one class of heterogeneous reactions, namely the OH oxidation of saturated organic particles.[9–20] These studies determined that, as observed in the gas phase, the reaction proceeds *via* H abstraction by the OH radical to form an alkyl radical (eqn (1)).[9–18] In the presence of O_2, the alkyl radical is rapidly transformed to a peroxy radical intermediate, which can react with another peroxy radical to form alkoxy radicals or higher molecular weight oxygenated products such as alcohols and ketones (*i.e.* functionalization).[9–13,15,16] As more oxygenated functional groups are added to the carbon backbone, volatilization becomes a significant loss channel for particulate organic matter presumably due to increased rates of alkoxy radical formation.[10–13,15,16] Alkoxy radicals can dissociate *via* C–C bond cleavage (*i.e.* fragmentation) into higher volatility lower molecular weight oxidation products that can evaporate from the particle, leading to a net reduction in particle mass.[10–13,15,16,18] The formation and dissociation rates of these alkoxy radicals are highly dependent on the molecular structure, with linear molecules undergoing significantly less fragmentation than branched molecules.[12,20]

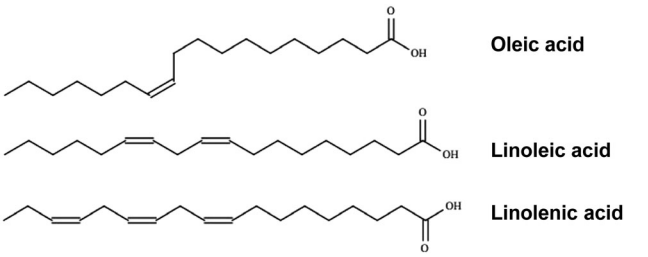

Fig. 1 Chemical structures of the unsaturated fatty acids used in this study: oleic acid, linoleic acid and linolenic acid.

Unlike the OH oxidation of saturated organic particles, there are few studies on the reaction of gas phase OH radicals with condensed phase unsaturated organic compounds. Studies of the reaction of OH radicals with alkene monolayers reveal that the reaction is fast and proceeds *via* OH addition to the C=C double bond (eqn (2)).[21,22] However, little is known about the oxidation products and the reaction pathways taken by the hydrocarbon radical intermediates to form these oxidation products.

In this work we present an in-depth investigation on the heterogeneous OH oxidation of unsaturated organic particles. The single-component unsaturated organic particles used in this study are oleic acid (OA, $C_{18}H_{34}O_2$), linoleic acid (LA, $C_{18}H_{32}O_2$) and linolenic acid (LNA, $C_{18}H_{30}O_2$). The molecular structures of these unsaturated fatty acids are shown in Fig. 1. Oleic acid, linoleic acid and linolenic acid have the same C_{18} carbon backbone structure with one, two and three C=C double bonds, respectively. By studying fatty acids with different numbers of C=C double bonds, the role that multiple reactive sites have on controlling the heterogeneous reaction probability can be observed.

The reaction of gas phase OH radicals with sub-micron unsaturated fatty acid aerosol particles is measured in a photochemical flow reactor in which OH radicals are produced by the photolysis of hydrogen peroxide (H_2O_2) gas. A combination of real-time atmospheric pressure chemical ionization (APCI-MS) and electron impact (EI-MS) aerosol mass spectrometry is used to examine the underlying reaction mechanism (*i.e.* OH addition) and the rates at which OH radicals react with unsaturated organic particles. APCI-MS is used to measure effective uptake coefficients and identify reaction products, while EI-MS is used to probe the changes in particle mass and elemental composition. The effect that O_2, H_2O_2 and OH concentrations have on the effective uptake coefficients is investigated to formulate a plausible reaction mechanism.

This work builds on our previous work on the heterogeneous kinetics and chemical mechanism (*i.e.* H abstraction) of the radical-initiated oxidation of saturated organic particles. In our previous studies on the OH- and Cl-initiated oxidation of saturated organic particles, we showed that the reaction, in the presence of O_2, proceeds sequentially *via* the addition of one oxygenated functional group per reactive loss of particle phase molecular species (*i.e.* functionalization) at the initial stages of oxidation.[7,9,13,15] As the saturated organic particle

becomes more oxygenated, fragmentation reactions become more important, resulting in volatilization becoming a significant loss channel for particulate organic matter.[12,13,15] We also showed that particle-phase secondary chain reactions, which depend on the concentrations of radical initiators and chain propagators and terminators, could dramatically alter reaction rates and product formation kinetics.[7,9] This present work is aimed at understanding the heterogeneous kinetics and chemical mechanism (*i.e.* OH addition) of the OH-initiated oxidation of unsaturated organic particles, as well as to ascertain the roles that secondary chain chemistry, functionalization and fragmentation reaction pathways play in governing the oxidative transformation of an unsaturated organic particle's physicochemical properties.

2. Experiment

The experimental setup is shown in Fig. 2. An atmospheric pressure flow reactor is used to investigate the heterogeneous reaction of OH radicals with unsaturated fatty acid particles. Aerosol particles are formed by homogeneous nucleation in a 0.35 L min^{-1} nitrogen (N_2) stream flowing through a ~45 cm long Pyrex tube containing the unsaturated fatty acid. The tube is heated in a furnace to ~105 °C producing a lognormal particle size distribution. The particle flow is then passed through an annular denuder containing activated charcoal to remove any residual gas phase organic compounds that may be formed in the tube furnace. The mean surface-weighted diameter and geometric standard deviation of the unsaturated fatty acid particles are ~125 and ~1.2 nm, respectively. The relative humidity within the flow reactor is fixed at 30% by introducing 0.3 L min^{-1} of N_2 through a water bubbler. In contrast to our previous work on the OH-initiated oxidation of saturated organic particles where OH radicals are generated *via* the photolysis of ozone (O_3) in the presence of humidified N_2,[9,12,13,15,17,18] here OH radicals are generated *via* the photolysis of H_2O_2 gas. O_3 is not used here since it can react with the C=C double bonds of the acids.

A stream of N_2–H_2O_2 mixture is introduced into the reactor by passing 0.1 to 0.22 L min^{-1} N_2 through an additional bubbler, which is packed with a 50 : 50 mixture of urea–hydrogen peroxide (UHP) and sand heated to 50 °C. As shown by Ball *et al.*, a steady stream of H_2O_2 gas is produced when solid UHP crystals are heated to a fixed temperature.[23] Additional flows of N_2, O_2 and a trace quantity of reference compound hexane (~150 ppb hexane in the flow reactor) are also added, to give a total flow rate of 1 L min^{-1} entering the flow reactor. The concentrations of O_2 reported here are flow ratios (*i.e.* volume concentrations). For example, 10% [O_2] is obtained when 0.1 L min^{-1} of the total 1 L min^{-1} flow is O_2. For the experiments performed without O_2, a scrubber (0.75 L Supelpure-O trap) is placed in the nitrogen lines to reduce the residual oxygen levels in the reactor, which are estimated to be less than 0.05%.

The gas and particle flows are mixed and introduced into a 1.7 m long, 6.15 cm inner diameter quartz flow reactor. OH radicals are generated along the length of the flow reactor using four continuous output 130 cm long Hg (λ = 254 nm) lamps placed outside and along the length of the flow reactor. The flow reactor is actively cooled using pressurized air directed perpendicularly at three points along the length of the flow reactor. The total flow rate going through the flow reactor is 1 L min^{-1}. Based on the illuminated portion of the flow reactor, this corresponds to an estimated reaction time of 232 s. The OH concentration is controlled by adjusting the photon flux of the Hg lamps (*i.e.* adjusting the voltage supplied to the Hg lamps) and/or the H_2O_2 concentration in the flow reactor. The H_2O_2 concentration in the flow reactor can be varied by either changing the temperature of the UHP–sand mixture or by changing the flow rate of N_2 gas passing through the bubbler containing the UHP–sand mixture. OH concentrations in the flow reactor range from 8×10^7 to 2×10^9 molec cm^{-3}.

Upon exiting the reactor, a fraction of the flow is sampled by an atmospheric pressure ionization triple quadrupole time-of-flight mass spectrometer (API-QTOF-MS, SCIEX model QSTAR XL) equipped with an atmospheric pressure chemical ionization (APCI) source to measure the molecular composition of the aerosol. The commercial APCI source is modified in order to allow for the direct introduction of aerosol. The aerosol stream enters the mass spectrometer through a 0.4 cm inner diameter quartz tube that is surrounded by a heater. The inner wall of the quartz tube is maintained at a temperature of ~200 °C to completely vaporize the aerosol. The resulting aerosol vapor exits the quartz tube and enters the ionization region, where the molecules are ionized under atmospheric conditions by chemical ionization induced by a corona discharge operating at 3 kV. As demonstrated by Warscheid *et al.*, depending on whether a positive or negative voltage is applied to the APCI source's corona discharge, stable $[M + H]^+$ and $[M - H]^-$ ions can be formed in the positive-ion and the negative-ion mode, respectively.[24] These ions are produced by gas phase ion–molecule reactions between charged reactant ions and neutral analyte molecules (M). The APCI mass spectra of the unsaturated fatty acids are detected in the negative ion mode (resolving power ~ 6000 at *m*/*z* 300). Calibrations are done prior to kinetic measurements to ensure that the ion signal is linearly proportional to the aerosol mass concentration.

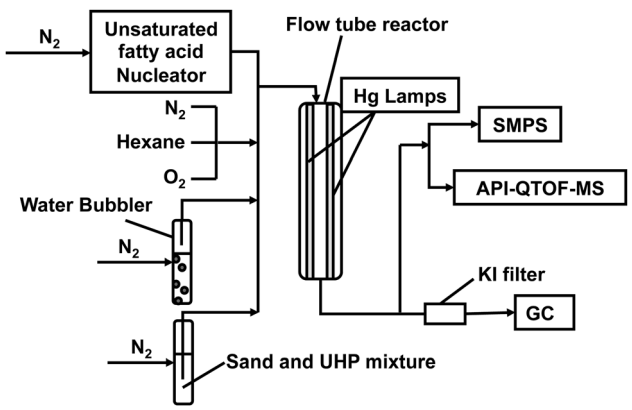

Fig. 2 Schematic of the experimental setup used to measure the OH reaction of unsaturated fatty acid aerosol.

For selected experiments, a high-resolution time-of-flight electron impact (EI) aerosol mass spectrometer (HR-ToF-AMS, Aerodyne Research Inc.) is used to determine the average oxygen-to-carbon (O/C) and hydrogen-to-carbon (H/C) elemental molar ratios of the aerosol.[25–28] At the mass resolution of the HR-ToF-AMS ($\sim$4300),[27] all of the ions in the mass spectrum can be identified, allowing for the determination of the relative abundances of C, H, and O in the sampled aerosol stream. Since the elemental ratios determined from EI need to be corrected for chemical biases that arise from ion fragmentation within the mass spectrometer,[25,26] the recommended correction factors of 0.75 for O–C and 0.91 for H–C are used for these measurements.

A fraction of the remaining flow is sampled by a gas chromatograph (GC) equipped with a flame ionization detector (SRI model 8610C) to monitor the loss of the gas phase reference compound hexane, which reacts with OH radicals at a rate constant of 5.2×10^{-12} cm^3 molec^{-1} s^{-1}.[29] Particles and H_2O_2 are removed prior to the GC measurement using a particle filter and a potassium iodide (KI) trap, respectively. For the detection of hexane, the flow is pre-concentrated in a Tenax™-GR adsorbent trap for 3 min before analysis. The GC monitors the decay of the hexane concentration during the reaction and is used to compute the average OH exposure ([OH] $\times$ time) using a relative rate approach described previously by Hearn *et al.*[19] and Smith *et al.*[13]

A scanning mobility particle sizer (SMPS, TSI model 3936) is used to measure the particle size distribution. An ozone monitor (2B Technologies Model 202), using an optical absorption cell at 254 nm, is used to determine the concentration of H_2O_2 in the flow reactor prior to reaction. To obtain H_2O_2 concentrations using this instrument, the measurements are corrected for the difference in the absorption cross-sections of O_3 and H_2O_2 at 254 nm.

For the experiments conducted to determine how [H_2O_2] and [O_2] in the reactor alter the reaction rate, the OH exposure is changed by keeping the total flow rate (*i.e.* reaction time) constant and changing the average OH concentration in the reactor by adjusting the photon flux of the Hg lamps and hence the photolysis rate of H_2O_2. Alternatively, for the measurements made to determine how the reaction rate depends on the absolute [OH] in the reactor, the OH exposure is changed by adjusting the reaction time instead of the photon flux of the Hg lamps. This is done by keeping the total flow rate fixed and moving an opaque curtain along the length of the flow reactor, as described by Liu *et al.*[7] This changes the illuminated reaction region and hence the reaction time. Analogous to the setup used by Liu *et al.*,[7] a constant H_2O_2 photolysis rate along the illuminated length of the flow reactor will result in a uniform concentration of OH radicals in the flow reactor. This leads to the OH exposure being linearly proportional to the residence time of the aerosol in the illuminated region of the reactor.

The rate constant for the heterogeneous reaction of unsaturated fatty acid particles with OH radicals is quantified by measuring the decay in the relative intensities of the unsaturated fatty acid ion signal in the mass spectrum as a function of OH exposure. The rate constant (k_{UFA}) for the OH reaction of unsaturated fatty acid aerosol is determined using the standard relative rate methodology described by Hearn *et al.*[19] and Smith *et al.*[13] The normalized decay of unsaturated fatty acid in the particle phase is,

$$\frac{[\mathrm{UFA}]}{[\mathrm{UFA}]_0} = \exp\left(-k_{\mathrm{UFA}}\langle \mathrm{OH}\rangle_t \cdot t\right) \quad (3)$$

where [UFA] and [UFA]$_0$ are the final and initial concentrations of the unsaturated fatty acid in the particle phase, respectively. The OH exposure ($\langle \mathrm{OH}\rangle_t \cdot t$) is obtained from the difference in hexane concentration measured before and after the reaction.

Assuming that k_{UFA} is independent of [OH], [UFA]/[UFA]$_0$ can be plotted against $\langle \mathrm{OH}\rangle_t \cdot t$ and fit to an exponential function to determine k_{UFA}. Using the formalism developed by Smith *et al.*, the effective uptake coefficient (γ_{OH}^{UFA}), defined as the fraction of OH collisions with the unsaturated fatty acid molecules in the particle phase that results in a reaction, can be expressed as,[13]

$$\gamma_{\mathrm{OH}}^{\mathrm{UFA}} = \frac{4 \cdot k_{\mathrm{UFA}} \cdot D_{\mathrm{surf}} \cdot \rho_0 \cdot N_{\mathrm{A}}}{\bar{c} \cdot 6 \cdot M_{\mathrm{UFA}}} \quad (4)$$

where D_{surf} is the mean surface-weighted particle diameter, ρ_0 is the initial unsaturated fatty acid density, N_A is Avogadro's number, $\bar{c}$ is the mean speed of gas phase OH, and M_{UFA} is the molar mass of the unsaturated fatty acid.

This formulation (eqn (4)) of the effective uptake coefficient assumes that the unsaturated fatty acid decay rate is directly proportional to the concentration of the unsaturated fatty acid in the particle.[13] Since monolayer studies have shown that the OH + alkene reaction is fast,[21,22] it is assumed that the heterogeneous OH reaction of the unsaturated fatty acid particle should be a fast surface reaction,[30] thus resulting in an exponential decay of the particle phase unsaturated fatty acid as a function of OH exposure.[13] The validity of this assumption will be discussed in Section 3A.

In addition, eqn (4) also assumes that the particle is internally well-mixed on the timescale of the reaction (*i.e.* mixing in the particle is sufficiently fast such that unreacted unsaturated fatty acid molecules are continuously replenished at the particle surface). The estimated timescale for the reactive loss of the acids (*i.e.* the ratio of the unsaturated fatty acid decay constant ($1/k_{UFA}$) to the average [OH] in the reactor) is several orders of magnitude ($\sim 7 \times 10^6$) longer than the mixing time in the particle.[31] Therefore the reaction is not limited by the diffusion of unsaturated fatty acid molecules to the particle surface on the timescale of the reaction.

3. Results and discussion

In Section 3A, the products and kinetics of the reaction of unsaturated fatty acid particles with OH radicals in the presence of O_2 are discussed. Elemental mass spectrometric analysis is presented in Section 3B to show how the average particle chemical composition and mass evolve during the reaction. In Section 3C, the roles that [O_2], [H_2O_2] and [OH] play in influencing reaction rates are explored. A proposed reaction mechanism is presented in Section 3D. The kinetic

evolution of the unsaturated fatty acids and their reaction products is discussed in Section 3E.

A. Reaction products and kinetics

APCI-MS is used to identify reaction products and measure effective uptake coefficients. The mass spectrum of unreacted linoleic acid particles is shown in Fig. 3a. Before reaction, the mass spectrum is dominated by the deprotonated linoleic acid molecular ion ($[M - H]^-$) at m/z 279, with very few lower molecular weight ions observed. Similar mass spectra are also observed for oleic acid and linolenic acid aerosol before reaction, where the mass spectrum is dominated by the deprotonated oleic acid (m/z 281) and linolenic acid (m/z 277) molecular ions, respectively (Fig. S-1a and S-2a in ESI†). This is consistent with a study by Hoffmann *et al.* where deprotonated molecular ions of various small carboxylic acid ($<C_{10}$ acid) aerosols are detected in the negative-ion APCI mode using a modified APCI ion source.[32] They determined that these species, being Brønsted acids, are highly sensitive towards chemical ionization and form stable deprotonated molecular ions upon ionization due to the loss of the acidic hydrogen atom. Although Hoffmann *et al.* detected acid dimers in their study,[32] no acid dimers are detected above the background signal here in the negative ion mode (Fig. 3a).

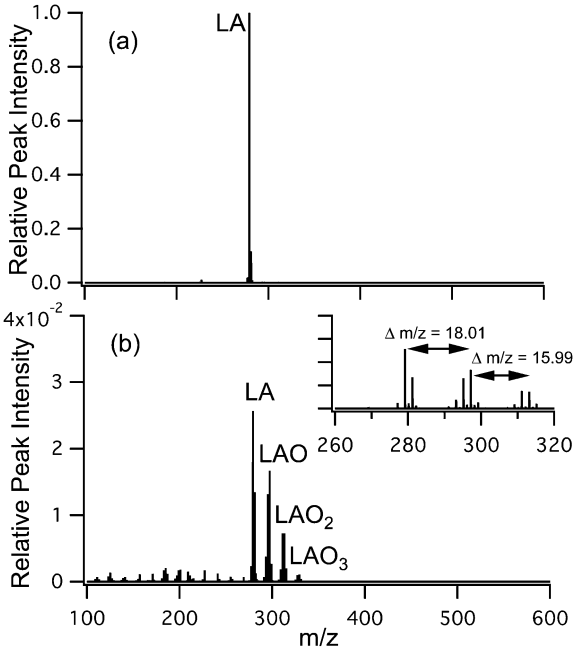

Fig. 3 The negative-ion APCI mass spectrum of linoleic acid (LA) particles from m/z 100 to 600. No peaks are observed above the background at masses lower than m/z 100. (a) Before reaction, the main peak observed in the spectrum is the linoleic acid parent ion ($[M - H]^-$, m/z 279). (b) After reaction with OH radicals ($\sim 2.3 \times 10^{11}$ molecules cm^{-3} s) at $[H_2O_2]$ = 20.7 ppm and $[O_2]$ = 10%, the linoleic acid peak intensity decreases and higher molecular weight oxygenated reaction products are formed. The groups of higher molecular weight oxygenated reaction products are denoted as LAO, LAO_2 and LAO_3, respectively, to denote the number of oxygen atoms added to the linoleic acid molecule. The inset shows the exact mass difference from the linoleic acid parent ion to the main peak in each group of reaction products. The mass spectra are normalized to the initial linoleic acid peak intensity before reaction.

Given the APCI-MS background signal (2 to 3 counts per s) here, peaks that are $<0.1\%$ of the unreacted unsaturated fatty acid molecular ion intensity cannot be detected using this MS technique. The absence of acid dimer peaks in the mass spectrum indicates that either acid dimers are not present in these C_{18} unsaturated fatty acid particles, or the acid dimers are not efficiently ionized by the APCI ion source, or thermal vaporization of the aerosol dissociates these dimeric species prior to ionization.

The reaction of OH with unsaturated fatty acid particles is expected to proceed *via* OH addition to the C=C double bond to form a hydroxyalkyl radical.[1–6,21,22] The heterogeneous reaction of OH radicals with unsaturated fatty acid particles is measured in the presence of 10% $[O_2]$. The mass spectrum of reacted linoleic acid is shown in Fig. 3b. Upon exposure to OH radicals ($\sim 2.3 \times 10^{11}$ molecules cm^{-3} s), the linoleic acid molecular ion peak decreases in intensity and the formation of higher molecular weight reaction products are observed. The reaction products appear in groupings of 5 to 6 peaks spaced by $\Delta m/z \sim 16$ to 18. The first group of peaks is centered at m/z 297. Based on the exact mass difference from the linoleic acid molecular ion peak, this product peak corresponds to the addition of one O atom and two H atoms.

The appearance of higher molecular weight reaction products centered at m/z 297 can be explained by a reaction mechanism in which some of the hydroxyalkyl radicals abstract a H atom from a neighboring linoleic acid molecule to form these resulting reaction products. This observation of H abstraction by the radical intermediate (*i.e.* hydroxyalkyl radical) from the molecular species (*i.e.* linoleic acid) is consistent with previous studies on the radical-initiated oxidation of unsaturated organic particles.[33,34] For example, from a recent study by Zhao *et al.* on the NO_3 oxidation of unsaturated fatty acid particles, there is evidence that a H atom is abstracted from a neighboring unsaturated fatty acid molecule by the nitroalkyl radical formed from the initial NO_3 addition to the C=C double bond.[34] In the case of the OH oxidation of saturated organic particles, Ruehl *et al.* has observed evidence of inter-molecular H abstraction by alkoxy radical intermediates in their study on the OH + squalane reaction.[20] However inter-molecular H abstraction by alkyl radicals formed from the initial H atom abstraction by the OH radical is not observed since this reaction does not lead to a measurable loss of the molecular species.

As shown in Fig. 3b, the product peaks in each successive group (centered at m/z 313 and 329 *etc.*) are separated by $\Delta m/z \sim 16$. Based on the masses of the reaction products within the second and third groupings of higher molecular weight reaction products, it appears that these groups of reaction products correspond to the multiple additions of O atoms to produce carbonyls and alcohols. However, it is difficult to draw quantitative conclusions about the relative populations of specific species (*e.g.* alcohols *vs.* ketones) within the same group of peaks based on the relative peak intensities in the mass spectrum, since the fragmentation patterns and ionization cross sections depend on the identity of the parent molecule. For simplicity, the three groups of higher molecular weight oxygenated reaction products are labeled as LAO, LAO_2 and

LAO_3 to denote the number of oxygenated functional groups (*i.e.* alcohols and ketones) that are added to the original linoleic acid molecule, as shown in Fig. 3b. Similar mass spectra are also observed for oleic acid and linolenic acid aerosol after reaction (Fig. S-1b and S-2b in ESI†), where the first group of higher molecular weight reaction products is separated from the unsaturated fatty acid molecular ion peak by $\Delta m/z \sim 18$ and the successive groups of higher molecular weight reaction products are separated by $\Delta m/z \sim 16$.

Based on the mass spectrum of reacted linoleic acid particles shown in Fig. 3b, no peaks are detected above the background signal at masses larger than m/z 350. Additionally no peaks are observed above the background at masses larger than m/z 350 for reacted oleic acid and linolenic acid particles (Fig. S-1b and S-2b in ESI†). This indicates that either higher molecular weight oligomeric products are not formed, or the conditions in the APCI source are unfavorable for the direct detection of these higher molecular weight oligomeric products.

As shown in Fig. 3b, there are peaks present in the mass spectrum of reacted linoleic acid particles that have masses smaller than that of linoleic acid. Some of these peaks are fragments from the ionization of the linoleic acid parent ion as they also appear in the mass spectrum of unreacted linoleic acid (Fig. 3a) and display the same kinetic behavior as the linoleic acid parent ion. The remaining peaks, however, follow the kinetic behavior of the higher molecular weight reaction products, and these are either fragments produced during the ionization of these higher molecular weight reaction products or are lower molecular weight products of fragmentation reactions that occur in parallel with functionalization reactions. Similar peaks at the lower masses for reacted oleic acid and linolenic acid particles are also observed (Fig. S-1b and S-2b in ESI†).

The decays in the relative intensities of the unsaturated fatty acid ion peaks in the mass spectrum are measured as a function of OH exposure in order to determine the effective uptake coefficient. For this set of measurements, the OH exposure is changed by varying the photon flux of the Hg lamps while keeping the reaction time and $[H_2O_2]$ constant. Shown in Fig. 4a are the normalized decay curves for the three unsaturated fatty acids ($[UFA]/[UFA]_0$) (*i.e.* oleic acid, linoleic acid and linolenic acid) *versus* OH exposure in the presence of 10% $[O_2]$ at 20.7 ppm $[H_2O_2]$. The decays of the unsaturated fatty acids' ion signals with OH exposure are fit using an exponential function described by eqn (3). Since a fast surface reaction would result in an exponential decay of the particle phase unsaturated fatty acid as a function of OH exposure, the exponential decays confirm our original assumption that the reaction rate of the unsaturated fatty acid is directly proportional to the concentration of unsaturated fatty acid in the particle and the chemical transformation of the particle is initiated by a reaction between a OH radical and the unsaturated fatty acid molecular species at the particle surface. Furthermore, the rate coefficient is observed to vary linearly as the inverse particle diameter (as shown for oleic acid in Fig. S-3 in the ESI†) which is further confirmation that the reaction occurs at the aerosol surface.

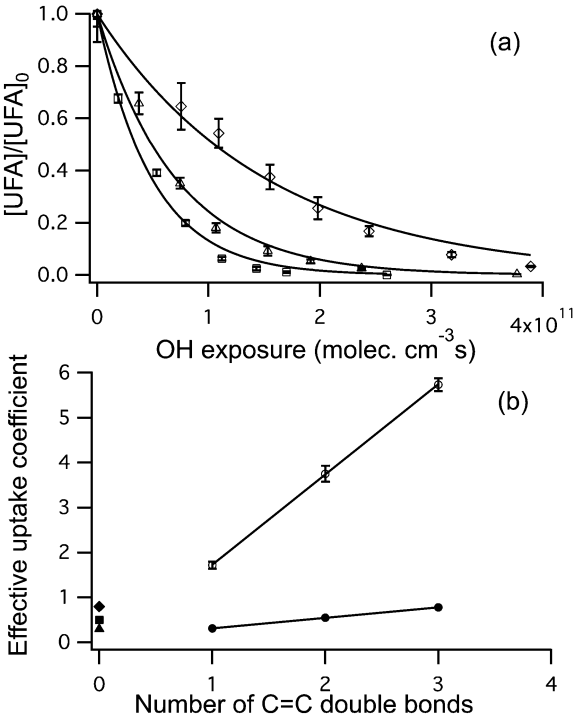

Fig. 4 (a) Normalized kinetic decay of oleic acid (◊), linoleic acid (△) and linolenic acid (□) measured as a function of OH exposure at $[H_2O_2]$ = 20.7 ppm and $[O_2]$ = 10%. The uncertainties represent the standard deviations of each measurement. The decay curves are fit using single exponential functions (solid lines). (b) Effective uptake coefficients of the unsaturated fatty acids (○) expressed as a function of the number of C=C double bonds at $[H_2O_2]$ = 20.7 ppm and $[O_2]$ = 10%. Uptake coefficients measured by Zhao *et al.*[34] for the NO_3 oxidation of unsaturated fatty acids (●) are also expressed as a function of the number of C=C double bonds. These two data sets are fit using a linear function $mx + c$ (solid line) where m is slope and c is the y-intercept, as described in the text. Uptake coefficients measured by Smith *et al.*,[13] Wilson *et al.*,[15] and McNeill *et al.*[10] for the OH oxidation of squalane (▲), dioctyl sebacate (■), and palmitic acid (◆) are also shown.

The decay constants, k_{UFA}'s obtained from the exponential fits to the three decay traces, are used to compute the effective uptake coefficients of the three unsaturated fatty acids using eqn (4). The effective uptake coefficients for oleic acid, linoleic acid and linolenic acid measured at 10% $[O_2]$ and 20.7 ppm $[H_2O_2]$ are 1.72 ± 0.08, 3.75 ± 0.18 and 5.73 ± 0.14 respectively. The effective uptake coefficients are larger than 1, which indicates that more than one particle phase unsaturated fatty acid molecule is lost for every OH-particle collision, providing clear evidence for particle-phase secondary chain chemistry. Due to unknown amounts of secondary chemistry, the effective uptake coefficients reported here are not corrected for gas phase diffusion.

Another possible explanation for the large effective uptake coefficients is the formation of particle phase OH radicals from the photolysis of H_2O_2 dissolved in the particle. These particle phase OH radicals may react with the unsaturated fatty acid molecules without escaping from the particle to be detected by the gas phase tracer. To evaluate the importance of this reaction channel, the production rate of particle phase OH radicals

in an oleic acid particle is estimated. While the Henry's law constant for H_2O_2 dissolved in an oleic acid is not known, the Henry's law constant for H_2O dissolved in an oleic acid particle is 70 M atm^{-1}.[35] Assuming that the Henry's law constant for H_2O_2 is also 70 M atm^{-1}, there are $\sim$456 H_2O_2 molecules in a 100 nm diameter oleic acid particle when the concentration of gas phase H_2O_2 in the flow reactor is 20.7 ppm. Under our experimental conditions (Hg lamp flux *etc.*), particle phase OH radicals are produced in a 100 nm diameter oleic acid particle at a rate of $\sim$2 OH radicals s^{-1}. In comparison, the collision frequency of gas phase OH radicals with the surface of a 100 nm diameter oleic acid particle is $\sim$3300 collision s^{-1} when the average gas phase OH concentration in the flow reactor is 7×10^8 molec cm^{-3}. This suggests that the production rate of particle phase OH radicals in the particle is $\sim$1700 times slower than the collision frequency of gas phase OH radicals with the particle surface. Since this source of particle phase OH radicals appears to be small compared to the gas phase source, we expect its contribution to the reaction to be minimal. It is more likely that particle-phase secondary chain reactions that accelerate the reactive loss of the unsaturated fatty acid molecules are responsible for the large effective uptake coefficients measured here.

Ruehl *et al.*[20] and Hearn *et al.*[36] have previously shown that molecular structure, thermodynamic phase and chemical functionality can influence the overall reactivity of organic particles. Here the large effective uptake coefficients can potentially be attributed to the chemical functionality (*i.e.* carboxylic acid) and molecular structure (*i.e.* linear) of these acids. X-ray diffraction studies on liquid oleic acid by Iwahashi and coworkers reveal that the oleic acid molecules form dimers through hydrogen bonding of the carbonyl oxygen and the acidic hydrogen.[37] By measuring the spacing between oleic acid molecules, Iwahashi *et al.* showed that these linear molecules line up close together and concluded that these oleic acid dimers are arranged in an orderly structure where the carboxylic acid groups of one dimer alternate with the terminal methyl groups of another dimer in the same lateral plane.[37] It is possible that the unsaturated fatty acid molecules are oriented in a similar fashion in the particle. This proposed orientation of the unsaturated fatty acid molecules within the particle could explain the rapid reaction of the unsaturated fatty acid molecular species since the close proximity of these molecules would enhance particle-phase secondary chain reactions that consume the molecular species. It is currently unclear how the reactivity of unsaturated organic particles differs between linear and branched unsaturated organic molecules. The effect of molecular structure on secondary chain chemistry, which may influence the unsaturated organic particle's overall reactivity and physicochemical properties (*e.g.* particle mass and elemental content), will be considered in a forth-coming paper.

Fig. 4b shows how the effective uptake coefficient changes as a function of the number of C=C double bonds present in the unsaturated fatty acid molecule. The effective uptake coefficients are a linear function of the number of C=C double bonds present in the unsaturated fatty acid molecule with a slope of 2, which is consistent with the addition of two reactive sites for OH addition and subsequent secondary chemistry with every addition of a C=C double bond along the C_{18} carbon backbone. Similarly, Zhao *et al.* found that the effective uptake coefficients for the NO_3 oxidation of unsaturated fatty acid particles increases linearly with the number of C=C double bonds (this data is also included in Fig. 4b).[34] The slope obtained by fitting the NO_3 + unsaturated fatty acid data is 0.24. The origin of this difference between the slopes obtained for the OH + unsaturated fatty acid and NO_3 + unsaturated fatty acid data is not clear but could potentially be attributed to the different secondary chain chemistry present in the two systems. However, based on the linear relationship between the effective uptake coefficients and the number of C=C double bonds in these two systems, the radical-initiated (*e.g.* OH and NO_3) oxidation of unsaturated organic particles appears to be driven primarily by radical addition to the C=C double bond and subsequent secondary chain chemistry.

Fig. 4b also shows that the effective uptake coefficients for the OH oxidation of unsaturated fatty acid particles are significantly larger than those of single-component saturated organic particles (*e.g.* squalane, dioctyl sebacate and palmitic acid).[10,13,15] This trend is consistent with monolayer studies by D'Andrea *et al.*,[21] where the alkene monolayer reacted with OH radicals at a faster rate than the alkane monolayer. Despite the similar trends observed in both organic particles and monolayer studies, it is important to note that since the quantity of particle-phase secondary chemistry (*i.e.* chain propagation length) occurring in the OH oxidation of unsaturated fatty acid particles is not known, we cannot ascertain the absolute difference in the heterogeneous reaction rates of OH radicals with the surface of unsaturated (*i.e.* OH addition reactions) and saturated (*i.e.* H abstraction reactions) organic particles based solely on the measured effective uptake coefficients.

B. Elemental analysis

The elemental composition of unsaturated fatty acid particles is measured using EI-MS to examine how the average chemical composition and mass of the particle change during the heterogeneous reaction. Fig. 5 shows how the average number of O atoms per acid molecule evolves as a function of unsaturated fatty acid lifetime (τ) at 20.7 ppm [H_2O_2] for 10% [O_2]. The kinetic lifetime represents the number of reactive events that an average unsaturated fatty acid molecule in the particle has undergone.[12,13,15] In radical-initiated heterogeneous reactions, these events are heterogeneous and homogeneous chain initiation and propagation reactions that consume the molecular species. At one lifetime, the number of reactive events equals the number of molecules in the particle. As shown by Smith *et al.*, the unsaturated fatty acid lifetime can be expressed as,[13]

$$\tau = k_{UFA} \cdot \langle OH \rangle_t \cdot t \quad (5)$$

where k_{UFA} is the measured rate constant and $\langle OH \rangle_t \cdot t$ is the measured OH exposure. The average number of O atoms present in the unsaturated fatty acid molecule is obtained by multiplying the average particulate oxygen content (normalized to the initial

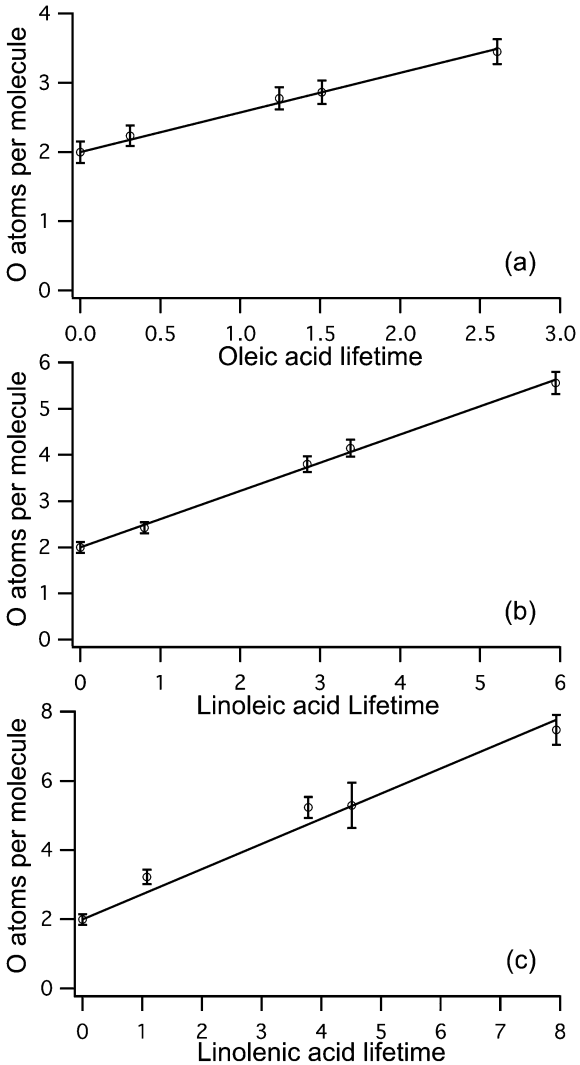

Fig. 5 The measured number of oxygen atoms per (a) oleic acid, (b) linoleic acid, and (c) linolenic acid molecule, as a function of unsaturated fatty acid lifetime at $[H_2O_2]$ = 20.7 ppm for $[O_2]$ = 10%. Lifetime represents the number of reactive events that an average unsaturated fatty acid molecule in the particle has undergone. At one lifetime, the number of reactive events that consume the molecular species equals the number of molecules in the particle. The uncertainties represent the standard deviations of each measurement. The data sets for the measured number of oxygen atoms per unsaturated fatty acid molecule are fit (lines) using the linear function 2 + *mx* (solid lines) where *m* is slope, as described in the text.

amount of particulate oxygen) with the initial number of O atoms in the unsaturated fatty acid molecule (N_O = 2). The average particulate oxygen content (the average number of O atoms in the particle phase, *n*O) is obtained by multiplying the elemental O/C ratio with the average particulate carbon content (the average number of C atoms in the particle phase, *n*C). As shown by Kroll *et al.*, *n*C is computed from the elemental O/C and H/C ratios and aerosol mass,[12]

$$nC = \frac{M}{12 + 16(O/C) + (H/C)} \quad (6)$$

where *M* is the particle mass and O/C and H/C are elemental ratios. The particle mass, which equals the sum of the masses of the elemental constituents in the particle (in this case, C, O and H), is determined from the product of the particle volume (measured by the SMPS) and the particle density, which is calculated from the ratio of the vacuum aerodynamic diameter (measured by the HR-ToF-AMS) and the mobility diameter (measured by the SMPS).[12,38] The O/C and H/C elemental ratios are obtained by analysis of the mass spectrum recorded by the HR-ToF-AMS.

Fig. 5 shows that the average number of O atoms in the acid molecule increases linearly with lifetime with slopes of 0.57 ± 0.02, 0.61 ± 0.01 and 0.73 ± 0.04 for oleic acid, linoleic acid and linolenic acid respectively. These slopes indicate that an average of 0.57 ± 0.02, 0.61 ± 0.01 and 0.73 ± 0.04 O atoms are added per reactive loss of oleic acid, linoleic acid and linolenic acid respectively. This is in contrast with previous results measured for the OH + squalane reaction, which yielded an average of one oxygenated functional group added per reactive loss of the alkane by the formation of alcohols and carbonyls.[13] Here one might expect an average of two O atoms added per reactive loss of the acid due to the formation of diols and hydroxycarbonyls from the reaction between hydroxyperoxy radicals, which are generated from the hydroxyalkyl radical + O_2 reaction. Instead the addition of less than one O atom per reactive loss of the acid indicates that OH addition to the C=C double bond is not the sole loss channel for the acid during these reactions. This suggests that the unsaturated fatty acid is consumed by other secondary reaction pathways that do not lead to an overall increase in the O content of the aerosol.

From the mass spectra of reacted unsaturated fatty acid aerosol, one possible secondary loss channel of the molecular species occurs *via* H abstraction by hydroxyalkyl radicals generated from the initial OH addition to the C=C double bond of the unsaturated fatty acid molecule (*i.e.* inter-molecular H abstraction). X-ray diffraction studies on liquid oleic acid show that oleic acid molecules form dimers that line up close together in the same lateral plane.[37] Assuming that the acid dimers are arranged such that the carboxylic acid groups of one dimer alternate with the terminal methyl groups of another dimer in the same lateral plane within the particle, it is likely that the hydroxyalkyl radical abstracts a H atom located along the unsaturated fatty acid's carbon chain.

H abstraction by hydroxyalkyl radicals will result in the formation of alkyl ($R^\bullet$) radicals. These $R^\bullet$ radicals could react with OH radicals or O_2 to subsequently form stable reaction products with oxygenated functional groups. It is also possible that these $R^\bullet$ radicals (and hydroxyalkyl radicals) participate in chain propagation chemistry by reacting with neighboring unsaturated fatty acid molecules (and their reaction products) *via* radical addition to the C=C double bond, thus triggering a radical chain polymerization mechanism that rapidly consumes the molecular species. To evaluate the relative importance of these reaction pathways, the overall rates of the $R^\bullet + O_2$ and $R^\bullet$ + C=C double bond reactions are estimated. For simplicity, only the homogeneous reaction of $R^\bullet$ radicals with O_2 dissolved in the particle is considered. For the

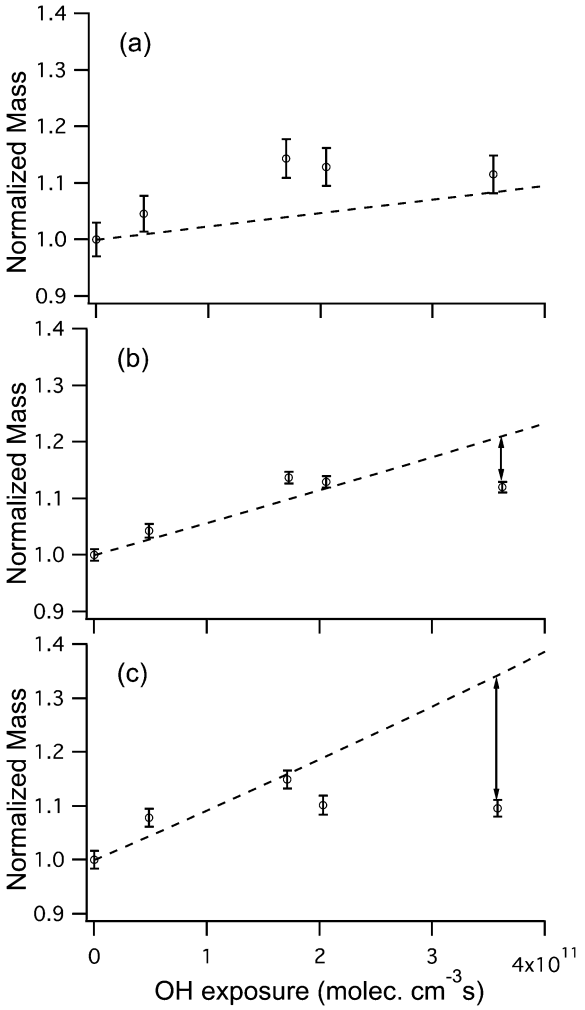

Fig. 6 Aerosol mass measurements (normalized to the initial mass per unreacted particle) of (a) oleic acid, (b) linoleic acid, and (c) linolenic acid, as a function of OH exposure at $[H_2O_2]$ = 20.7 ppm for $[O_2]$ = 10%. The uncertainties represent the standard deviations of each measurement. The measured data are compared with the particle mass predictions (dashed lines) based on measurements that an average of 0.57, 0.61 and 0.73 O atoms are added per reactive loss of oleic acid, linoleic acid and linolenic acid respectively, as described in the text. The degree of particle volatilization is the difference between the measured particle mass and the predicted mass (arrows).

homogeneous $R^\bullet + O_2$ reaction, the time dependent change in the concentration of $R^\bullet$ in a particle is,

$$\mathrm{Rate}_{R+O_2} = \frac{d[R^\bullet]}{dt} = k_{R+O_2} H_{O_2} [O_2][R^\bullet] \qquad (7)$$

where k_{R+O_2} is the rate constant for the homogeneous $R^\bullet + O_2$ reaction and H_{O_2} is the Henry's law constant for O_2 dissolved in the unsaturated fatty acid particle. While the Henry's law constant for O_2 in unsaturated fatty acid is not known, the Henry's law constant for O_2 dissolved in squalane is 0.18 (dimensionless ratio).[7,39] H_{O_2} is assigned a value of 0.18 in eqn (7). k_{R+O_2} is set to 8.5×10^{-16} cm^3 molec^{-1} s^{-1} in eqn (7), similar to the kinetic parameter used by Liu *et al.* in their kinetic model on the Cl reaction of squalane particles in the presence of O_2.[7] For the homogeneous $R^\bullet$ + C=C double bond reaction, the time dependent change in the concentration of $R^\bullet$ in a particle is given by,

$$\mathrm{Rate}_{R+C=C} = \frac{d[R^\bullet]}{dt} = k_{R+C=C}[C=C][R^\bullet] \qquad (8)$$

where $k_{R+C=C}$ is the rate constant for the homogeneous $R^\bullet$ + C=C double bond reaction. While the exact value of $k_{R+C=C}$ is not known from our measurements, polymer literature on radical chain polymerization involving alkyl radical addition to the C=C double bonds of olefins suggests that $k_{R+C=C}$ is typically in the range of 10^{-18} to 10^{-16} cm^3 molec^{-1} s^{-1}.[40] [C=C] is the concentration of C=C double bonds in the particle and is on the order of $\sim 10^{21}$ molec cm^{-3}. For the O_2 concentrations (10% $[O_2]$) used in the experiments reported here, dividing $\mathrm{Rate}_{R+C=C}$ (eqn (8)) by Rate_{R+O_2} (eqn (7)) yields,

$$\frac{\mathrm{Rate}_{R+C=C}}{\mathrm{Rate}_{R+O_2}} = \sim 10 \text{ to } 1000 \qquad (9)$$

This is an upper limit estimate of the rate analysis since the heterogeneous $R^\bullet + O_2$ reaction is not considered here.

The preceding rate analysis suggests that, for the particle size and experimental conditions used here, the reaction of $R^\bullet$ radicals with the C=C double bonds (*i.e.* oligomerization) of the unsaturated fatty acid molecules (and their reaction products) would be faster than the reaction of $R^\bullet$ radicals with O_2. These proposed radical chain polymerization mechanisms could potentially accelerate the reactive loss of the unsaturated fatty acid molecular species without increasing the O content of the aerosol. This reaction channel may explain the large effective uptake coefficients and observations that an average of less than one O atom is added per reactive loss of the acid. The proposed mechanisms are consistent with previous work by D'Andrea *et al.* on the OH + alkene monolayer reaction in the absence of O_2 where chemical changes in the alkene monolayer are attributed to a radical chain polymerization mechanism that leads to the formation of cross-linked polymeric alcohols.[21] The formation of polymers induced by the reaction of unsaturated organic compounds is not new, and it has been observed previously in condensed phase reactions.[41,42] Unfortunately, polymeric reaction products are not observed in the mass spectra of reacted unsaturated fatty acid particles, suggesting that the conditions in the APCI source may be unfavorable for the detection of such polymers.

Fig. 6 shows the measured particle mass (normalized to the mass of the unreacted particle) as a function of OH exposure measured at 20.7 ppm $[H_2O_2]$ and 10% $[O_2]$. The particle mass measurements are compared with predictions (shown as dashed lines in Fig. 6) based on measurements that an average of 0.57, 0.61 and 0.73 O atoms are added per reactive loss of oleic acid, linoleic acid and linolenic acid respectively. H atom addition/loss is not considered in the mass predictions due to the relatively minor mass contribution of H atoms ($\sim$1%) to the overall change in the particle mass. For each unsaturated fatty acid, the average particle mass increases at early OH exposures, which is consistent with an increase in particulate oxygen content as described above. For oleic acid, the measured

aerosol mass is larger than the predicted mass and could be attributed to a minor contribution from secondary organic aerosol formed by the oxidation of gas phase oleic acid. For linoleic acid and linolenic acid, the measured mass and predicted mass are similar at early OH exposures, indicating that reactions that add oxygenated functional groups to the particle (*i.e.* functionalization reactions) are important reaction pathways during the initial stages of oxidation, with fragmentation reactions being a minor reaction channel initially. The measured particle mass starts to decrease upon further reaction and deviates increasingly from the predicted mass with increasing OH exposure, signaling the formation of volatile reaction products that evaporate from the particle. These observations are consistent with previous works that show that fragmentation reactions increase in importance as the particle becomes more oxidized.[10–13,15,16]

C. Effective uptake coefficient *vs.* $[O_2]$, $[H_2O_2]$ and [OH]

The effective uptake coefficients of oleic acid, linoleic acid and linolenic acid are measured at different O_2, H_2O_2 and OH concentrations to determine how they influence the secondary chain chemistry. Fig. 7 shows the effective uptake coefficients of the unsaturated fatty acid particles as a function of $[O_2]$ in the flow reactor at 20.7 ppm $[H_2O_2]$. For each unsaturated fatty acid, the effective uptake coefficient decreases before leveling off when $[O_2]$ is increased. The effective uptake coefficients of oleic acid, linoleic acid and linolenic acid are found to be 2.10 ± 0.10, 4.13 ± 0.07 and 6.21 ± 0.17 respectively at 0% $[O_2]$, and decrease to 1.72 ± 0.08, 3.75 ± 0.18 and 5.73 ± 0.14 respectively at 10% $[O_2]$.

The decrease in the effective uptake coefficient with increasing $[O_2]$ is similar to the trend observed by Liu and coworkers in their study on the Cl reaction of squalane particles.[7] In the Cl + squalane reaction, Liu *et al.* found that the decrease in the effective uptake coefficient with increasing $[O_2]$ is due to the secondary chain chemistry being controlled by the competitive reaction rates of the squalane alkyl radicals with O_2 and the radical precursor Cl_2. In the absence of O_2, the squalane alkyl radicals react with Cl_2 to produce chlorinated reaction products and a Cl atom, which propagates the particle-phase secondary chain chemistry. This resulted in an increase in the depletion rate of the squalane molecular species and a corresponding increase in the effective uptake coefficient. When increasing amounts of O_2 are added to the reaction, the effective uptake coefficient decreases as the chain reaction slows since the squalane alkyl radicals react instead with O_2 to form peroxy radicals that subsequently react with other peroxy radicals to form terminal oxygenated products (*i.e.* chain termination).[7]

Since our results also show that the effective uptake coefficient decreases with increasing $[O_2]$, this suggests that the amount of particle-phase secondary chain chemistry in the OH reaction of unsaturated fatty acid particles is also controlled by $[O_2]$. In the absence of O_2, it is possible that the hydroxyalkyl radical formed from the initial OH addition to the C=C double bond participates in chain propagation, thus resulting in an increase in the reactive depletion rate of the unsaturated fatty acid molecular species and a corresponding increase in the effective uptake coefficient. When increasing amounts of O_2 are added to the reaction, the chain reaction slows since the hydroxyalkyl radicals can react instead with O_2 to form hydroxyperoxy radicals, which can react with another hydroxyperoxy radical to form terminal reaction products (*i.e.* chain termination). Therefore the inverse relationship between the effective uptake coefficients and $[O_2]$ in the OH reaction of unsaturated fatty acid particles appears to be the result of competitive reaction rates between chain propagation and termination reactions.

Liu *et al.*[7] and Renbaum *et al.*[43] have demonstrated that the radical precursor itself can act as a chain propagator or inhibitor that enhances or arrests reaction rates respectively. To determine how the radical precursor H_2O_2 influences reaction rates in the OH reaction of unsaturated fatty acid particles, the effective uptake coefficients of the unsaturated fatty acid particles are measured as a function of $[H_2O_2]$ in the flow reactor. Fig. 8 shows the effective uptake coefficients of oleic acid, linoleic acid and linolenic acid as a function of $[H_2O_2]$ at 10% $[O_2]$. The effective uptake coefficients of oleic acid, linoleic acid and linolenic acid are found to be 2.71 ± 0.17, 5.37 ± 0.24 and

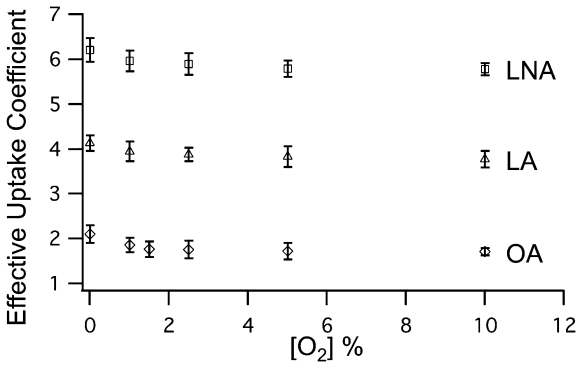

Fig. 7 Effective uptake coefficients as a function of $[O_2]$ for oleic acid (OA, ◊), linoleic acid (LA, △) and linolenic acid (LNA, □) at $[H_2O_2]$ = 20.7 ppm. The uncertainties represent the standard deviations of individual measurements made at each $[O_2]$.

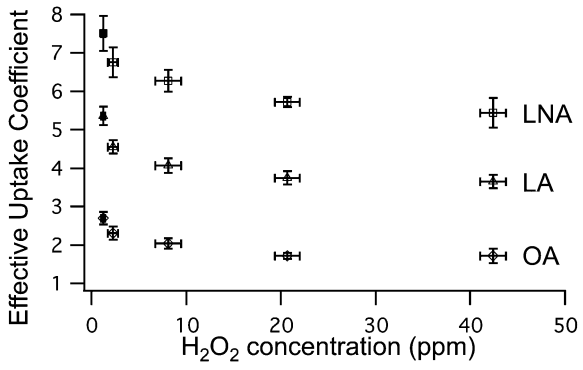

Fig. 8 Effective uptake coefficients as a function of $[H_2O_2]$ for oleic acid (OA, ◊), linoleic acid (LA, △) and linolenic acid (LNA, □) at $[O_2]$ = 10%. The uncertainties represent the standard deviations of individual measurements made at each $[H_2O_2]$.

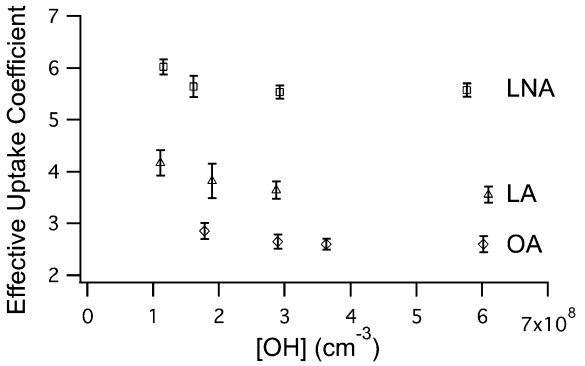

Fig. 9 Effective uptake coefficients as a function of absolute [OH] for oleic acid (OA, ◊), linoleic acid (LA, △) and linolenic acid (LNA, □) at $[H_2O_2]$ = 20.7 ppm and $[O_2]$ = 10%. The uncertainties represent the standard deviations of individual measurements made at each absolute [OH].

7.51 ± 0.46 respectively at 1.21 ± 0.23 ppm $[H_2O_2]$ and decrease to 1.72 ± 0.19, 3.66 ± 0.18 and 5.44 ± 0.39 respectively at 42.40 ± 1.35 ppm $[H_2O_2]$.

Although there is clear evidence that the radical precursor Cl_2 participates in chain propagation in the Cl reaction of squalane particles,[7] the chain propagation steps and the role of the radical precursor H_2O_2 in the chemistry of the OH + unsaturated fatty acid reaction is less apparent. The decrease in the effective uptake coefficient with increasing concentrations of the radical precursor H_2O_2 is inconsistent with the trend observed by Liu *et al.* in their study of the Cl reaction of squalane particles,[7] where the radical precursor Cl_2 acts as a chain propagator causing the effective uptake coefficient to increase with $[Cl_2]$. Instead, this inverse relationship between the effective uptake coefficient and $[H_2O_2]$ is more similar to the trend observed by Renbaum *et al.* in their study of the OH reaction of 2-octyldodecanoic acid particles,[43] where the effective uptake coefficient decreases with increasing concentrations of the radical precursor O_3. In that study, the effective uptake coefficients are described by a Langmuir-type isotherm, thus suggesting that O_3 impedes the OH reaction of 2-octyldodecanoic acid particles by adsorbing to the particle surface and blocking OH reaction sites at the particle surface. This causes the reaction rate to decrease with increasing $[O_3]$. Analogous to the OH reaction of 2-octyldodecanoic acid particles,[43] it is possible that H_2O_2 adsorbs to the unsaturated fatty acid particle surface and blocks OH reaction sites at the particle surface. As a result, the OH reaction of unsaturated fatty acid particles is slowed, thus causing the effective uptake coefficient to decrease with increasing $[H_2O_2]$.

Since H_2O_2 is the radical precursor in this system, it is also possible that the relationship between the effective uptake coefficient and $[H_2O_2]$ is correlated with the relationship between the effective uptake coefficient and absolute [OH]. To determine how the secondary chain chemistry depends on the absolute [OH] in the flow reactor, the effective uptake coefficients of the unsaturated fatty acid particles are measured as a function of absolute [OH]. Effective uptake coefficients are measured at fixed $[H_2O_2]$ and [OH] by changing the reaction time, and hence OH exposure, using an opaque curtain as described in Section 2. Fig. 9 shows the effective uptake coefficients of the unsaturated fatty acid particles as a function of [OH] at 20.7 ppm $[H_2O_2]$ for 10% $[O_2]$. For each unsaturated fatty acid, the effective uptake coefficient decreases when the absolute [OH] in the flow reactor increases.

The inverse relationship between the effective uptake coefficient and the absolute [OH] is similar to that observed by Slade *et al.* in their study of the OH reaction of levoglucosan, abietic acid, and nitroguaiacol solid substrates.[44] In that study, the decrease in the effective uptake coefficients with increasing [OH] is interpreted by a Langmuir–Hinshelwood model, which suggests that OH radicals collide and adsorb to the solid substrate surface before reacting. It is currently unclear how this mechanism can be applied to a liquid particle where the surface is continuously replenished with unreacted unsaturated fatty acid molecules.

Alternatively, since particle-phase secondary chain chemistry is present in this system, chain termination reactions involving OH radicals could explain the inverse relationship between the effective uptake coefficient and the absolute [OH]. In their study of the Cl reaction of squalane particles, Liu *et al.* found that the effective uptake coefficient decreases with increasing absolute [Cl].[7] The inverse relationship between the effective uptake coefficient and the absolute [Cl] is explained by the presence of chain termination reactions between two Cl atoms, as well as chain termination reactions between Cl atoms and squalane alkyl radicals. These chain termination reactions, which consume Cl atoms that would otherwise react with the squalane molecular species, compete with chain propagation reactions, thus slowing the chain reaction down and causing the effective uptake coefficient to decrease with increasing absolute [Cl]. Since our results also show that the effective uptake coefficient decreases with increasing absolute [OH], this suggests that chain termination reactions involving OH radicals could be responsible for the inverse relationship between the effective uptake coefficient and absolute [OH].

D. Reaction mechanism

Fig. 10 shows a possible reaction scheme for the OH reaction of unsaturated fatty acid particles. It is important to note that several of the reaction pathways shown in Fig. 10 can occur both at the particle surface (denoted as s in Fig. 10) as well as within the particle (denoted as p in Fig. 10). For example, hydroxyalkyl radicals generated from the initial OH addition to the C=C double bond (R1 in Fig. 10), can react homogeneously with O_2 dissolved in the particle *via* R4p in Fig. 10. Alternatively, the hydroxyalkyl radicals can react with O_2 heterogeneously through a reactive gas phase collision of O_2 at the particle surface *via* R4s in Fig. 10.

R1s is the heterogeneous reaction of a gas phase OH radical with an unsaturated fatty acid molecule at the particle surface that initiates the chemistry in the particle. Based on the reaction scheme shown in Fig. 10, chain propagation occurs through two possible chain cycling mechanisms. The first chain cycling mechanism occurs *via* R2p, where the hydroxyalkyl radical

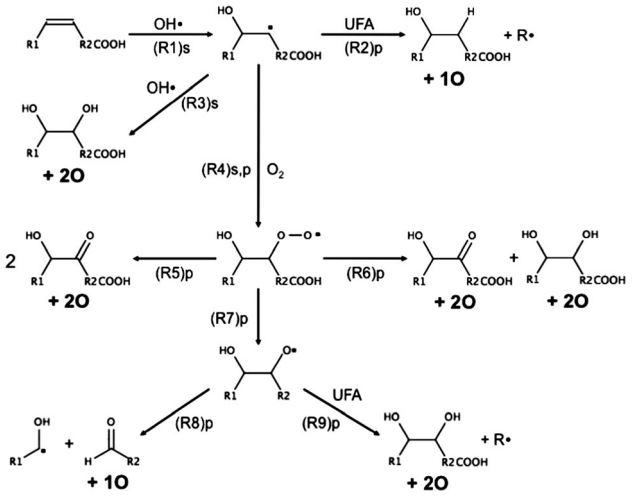

Fig. 10 Proposed reaction scheme for the OH oxidation of unsaturated fatty acid (UFA) particles. The letters s and p denote surface and particle phase reactions respectively. R• represents the generic alkyl radical formed by the abstraction of a hydrogen atom from an UFA molecule. The number of O atoms added to the unsaturated fatty acid molecule for the various reaction pathways are also shown.

abstracts a H atom from a neighboring unsaturated fatty acid molecular species in the particle to produce an alkyl (R•) radical and a stable reaction product with one additional oxygenated functional group. This channel would explain the formation of the LAO product peak shown for reacted linoleic acid aerosol in Fig. 3b, where this group of reaction products (centered at *m*/*z* 297) corresponds to the addition of one O atom and two H atoms.

The R• radical formed in R2p may react with OH to form a stable reaction product with an alcohol functional group. Alternatively, the R• radical may form a peroxy radical in the presence of O_2, which can then react *via* a number of reaction pathways (*e.g.* self-reaction) to subsequently form stable reaction products with oxygenated functional groups (not shown in Fig. 10). However, given that an average of less than one O atom is added per reactive loss of the acid, this suggests that the R• + OH and R• + O_2 reactions are not the sole reaction channels. As discussed in Section 3B, it is possible that the R• radical reacts with a neighboring unsaturated fatty acid molecule *via* radical addition to the C=C double bond. This reaction channel may potentially accelerate the reactive loss of the molecular species without increasing the O content of the aerosol.

The second chain cycling mechanism is proposed to occur *via* R9p in the presence of O_2. The hydroxyalkyl radical reacts heterogeneously (R4s) and homogeneously (R4p) with O_2 to form a hydroxyperoxy radical. As shown previously in condensed phase studies by Ingold *et al.*[45] and von Sonntag *et al.*,[46,47] the hydroxyperoxy radical can react with another hydroxyperoxy radical to form a tetroxide intermediate, which can rapidly dissociate to form hydroxyalkoxy radicals (R7p). The hydroxyalkoxy radical can then abstract a H atom from a neighboring unsaturated fatty acid molecular species in the particle to produce a stable reaction product with two added oxygenated functional groups and a R• radical (R9p), which can participate in chain propagation chemistry.

Based on the reaction scheme shown in Fig. 10, there are a number of reaction pathways that produce stable reaction products. One such reaction pathway occurs *via* R3s, where the hydroxyalkyl radical reacts heterogeneously with a gas phase OH radical to generate stable di-alcohol reaction products. This chain termination reaction pathway, which consumes OH radicals that would otherwise react with the unsaturated fatty acid molecular species, competes with chain propagation reactions, thus slowing the chain reaction down and causing the effective uptake coefficient to decrease with increasing absolute [OH]. Alternatively, in the presence of O_2, the hydroxyalkyl radical can react heterogeneously (R4s) and homogeneously (R4p) with O_2 to form a hydroxyperoxy radical, which can subsequently react with another hydroxyperoxy radical to form a tetroxide intermediate.[45–47] The tetroxide intermediate can dissociate to form two stable hydroxycarbonyl reaction products *via* R5p (*i.e.* Bennett–Summers mechanism) or stable di-alcohol and hydroxycarbonyl reaction products *via* R6p (*i.e.* Russell mechanism).[45–48] The tetroxide intermediate can also dissociate to form hydroxyalkoxy radicals (R7p).[45–47] The hydroxyalkoxy radical can then dissociate *via* C–C bond cleavage (R8p) to form stable lower molecular weight oxidation products.

Based on the reaction scheme shown in Fig. 10, reactions R2p, R3s, R5p, R6p and R9p produce stable higher molecular weight reaction products and are responsible for the addition of polar oxygenated functional groups to the unsaturated fatty acid particle with no change in the particulate carbon content (*i.e.* functionalization). These reactions are responsible for the increase in average particle mass at early OH exposures shown in Fig. 6. Conversely, R8p produces lower molecular weight reaction products *via* C–C bond cleavage along the carbon skeleton (*i.e.* fragmentation). These lower molecular weight reaction products have a higher vapor pressure than the unsaturated fatty acid molecular species and may evaporate from the particle. Since Fig. 6 shows that the average particle mass starts to decrease at higher OH exposures, this implies that R8p becomes increasingly important as the particle gets more oxidized.

It should be noted that the reaction scheme shown in Fig. 10 is only applicable to the multigenerational formation of reaction products formed *via* OH addition to the C=C double bond. Once all the C=C double bonds present in the organic particle have reacted, further OH oxidation of the organic particle is expected to take place *via* H abstraction by the OH radical, and the reaction scheme is expected to mirror that of the OH oxidation of saturated organic particles (not shown).

E. Kinetic evolution of the unsaturated fatty acids and their higher molecular weight reaction products

The kinetic evolution of the unsaturated fatty acids and their higher molecular weight reaction products are measured as a function of OH exposure to determine how the reactivity of the unsaturated fatty acids differs from their reaction products. In contrast to the radical-initiated oxidation of single-component

saturated organic particles where the kinetic evolution of the parent compound and its reaction products can be reasonably represented using a single rate constant,[7,9,13,15] the unsaturated fatty acids are expected to react significantly faster than their reaction products. This is because the reactivity of the unsaturated fatty acid towards OH radicals and secondary chain chemistry will be diminished as the C=C double bonds present in the C_{18} acid are consumed (and are replaced by C–C bonds). This is shown in Fig. 4b, where the effective uptake coefficient of the unsaturated fatty acids decreases dramatically with each removal of a C=C double bond (and replacing it with a C–C bond).

The kinetic evolution of linoleic acid and its first two groups of higher molecular weight oxygenated reaction products (LAO and LAO_2 in Fig. 3b) and the average number of O atoms per linoleic acid molecule *versus* OH exposure measured at 20.7 ppm [H_2O_2] for 10% [O_2] are shown in Fig. 11. Based on the reaction scheme shown in Fig. 10, LAO is made up solely of first generation reaction products formed from reaction R2p. In contrast, LAO_2 contains both first generation reaction products formed from reactions R3s, R5p, R6p and R9p, and second generation reaction products formed from the reaction of LAO with OH radicals.

The kinetic evolution of LAO and LAO_2 is compared with calculations based upon gas phase structure–activity relationships (SAR)[49] to identify similarities and/or differences between heterogeneous and gas phase reaction rates. SAR calculations[49] predict that the first and second generation products of linoleic acid react at rates that are ~40 and ~80% slower than linoleic acid respectively. The standard deviation for the SAR-estimated rate coefficients is not known. A kinetic model is used to simulate these SAR predictions of the kinetic evolution of linoleic acid, LAO and LAO_2 (shown as solid lines in Fig. 11). As shown in Fig. 11b and c, SAR predicts that LAO and LAO_2 would peak at OH exposures $\sim 8.8 \times 10^{10}$ and $\sim 1.9 \times 10^{11}$ molec cm^{-3} s, respectively. Since the LAO and LAO_2 products peak at OH exposures larger than those predicted by SAR, this indicates that LAO and LAO_2 are formed and react at much slower rates than that predicted by SAR calculations.

The deviation in the kinetic evolution of LAO and LAO_2 from SAR predictions can be explained by differences between the gas–particle interface and a homogeneous gas phase environment. In addition, the presence of particle-phase secondary chain reactions that accelerate the reactive depletion rate of the unsaturated fatty acid molecular species without forming higher molecular weight oxygenated reaction products can also contribute to these deviations. The high molecular density in the organic particle may enhance these radical chain cycling mechanisms, resulting in LAO and LAO_2 being formed at slower rates than that predicted by SAR.

To approximate the formation and reaction rates of LAO and LAO_2 relative to the reaction rate of linoleic acid, the kinetic evolution of LAO and LAO_2 is represented using a rate constant (k_{LA}') that is smaller than the measured rate constant (k_{LA}) for linoleic acid. For simplicity, the formation and reaction rate coefficients of both first and second generation products of linoleic acid are assumed to be k_{LA}'. Model fits to the LAO and LAO_2 experimental data using k_{LA}' are shown as dashed lines in Fig. 11b and c. By using a rate constant that is 60 ± 5% slower

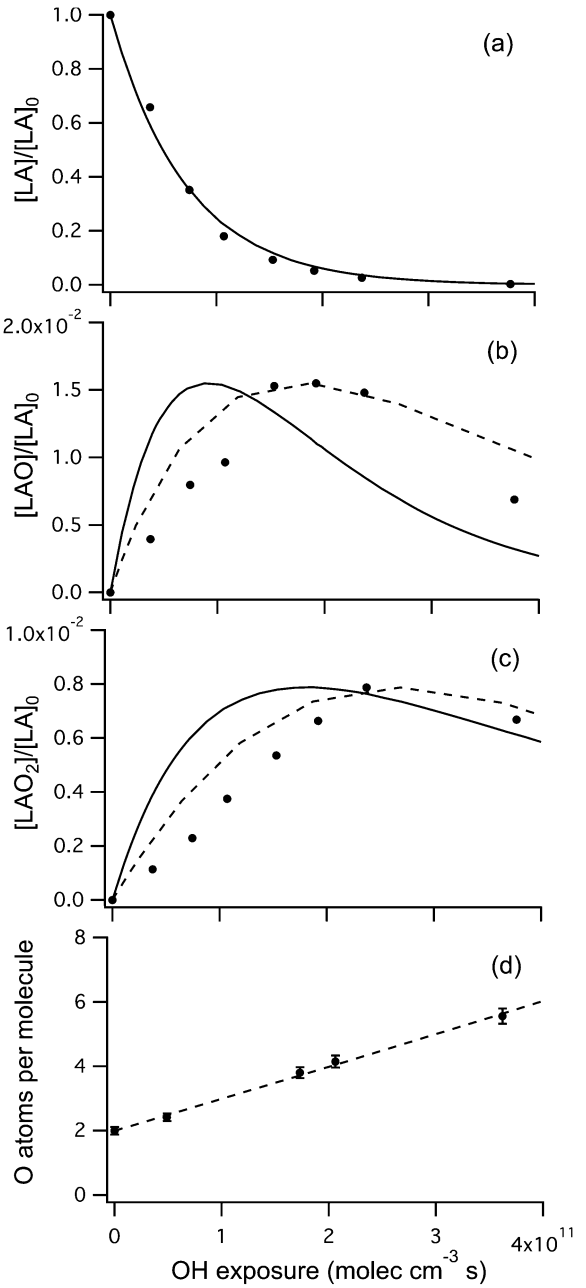

Fig. 11 (a) to (c) The kinetic evolution of linoleic acid, LAO and LAO_2 as a function of OH exposure at [H_2O_2] = 20.7 ppm for [O_2] = 10%. In panel (a), the decay of linoleic acid is fit using eqn (3) to obtain k_{LA} (solid line). In panels (b) and (c), the LAO and LAO_2 data sets are fit (dashed lines) using k_{LA}' (*i.e.* $k_{LA}' = 0.4 \times k_{LA}$) as described in the text. The solid lines in panels (b) and (c) are model predictions calculated using SAR, which serve as a comparison to the measured product evolutions. (d) Average number of oxygen atoms per linoleic acid molecule as a function of OH exposure at [H_2O_2] = 20.7 ppm for [O_2] = 10%. The uncertainties represent the standard deviations of individual measurements made at each OH exposure. The measured data are compared with predictions (dashed line) using k_{LA}' and the assumption that first generation higher molecular weight oxygenated reaction products with one and two added oxygenated functional groups are formed with equal probability.

than k_{LA} (*i.e.* $k_{LA}' = 0.4 \pm 0.05 \times k_{LA}$), the kinetic behavior of LAO and LAO_2 is captured by k_{LA}', as shown in Fig. 11b and c respectively.

To reconcile the kinetic evolution of the higher molecular weight oxygenated reaction products with the particulate oxygen content, the average number of O atoms per linoleic acid molecule is compared with model predictions in Fig. 11d. The model predictions (shown as a dashed line in Fig. 11d) are calculated using k_{LA}' and the assumption that first generation higher molecular weight oxygenated reaction products with one and two added oxygenated functional groups are formed with equal probability. As shown in Fig. 11d, the predicted particulate oxygen content calculated using k_{LA}' fits the experimental data well. Since k_{LA}' represents the kinetic evolution of LAO, LAO_2 and the particulate oxygen content experimental data well, this indicates that the formation and reaction of early generations of higher molecular weight products occur at rates $60 \pm 5\%$ slower than the reactive depletion of linoleic acid.

Similar calculations are performed on the kinetic evolution of oleic acid and linolenic acid and their first two groups of higher molecular weight reaction products and particulate oxygen content. In Fig. S-4 (ESI†), the kinetic evolution of oleic acid and its first two groups of higher molecular weight oxygenated reaction products (OAO and OAO_2) are compared with SAR calculations[49] (shown as solid lines in Fig. S-4 in the ESI†), which predict that OAO and OAO_2 react at rates $\sim$70% slower than oleic acid. As shown in Fig. S-4 (ESI†), the SAR calculations do not capture the behavior of OAO and OAO_2 completely. Instead, a rate constant that is $62 \pm 3\%$ slower than k_{OA} (*i.e.* $k_{OA}' = 0.38 \pm 0.03 \times k_{OA}$) is needed to account for the kinetic evolution of OAO and OAO_2 and average number of O atoms per oleic acid molecule (shown as dashed lines in Fig. S-4 in the ESI†).

In Fig. S-5 (ESI†), the kinetic evolution of linolenic acid and its first two groups of higher molecular weight oxygenated reaction products (LNAO and $LNAO_2$) are compared with SAR calculations[49] (shown as solid lines in Fig. S-5 in the ESI†), which predict that the first and second generation products of linolenic acid react at rates $\sim$30 and $\sim$60% slower than linolenic acid respectively. The SAR calculations do not capture the behavior of LNAO and $LNAO_2$ completely, and a rate constant that is $54 \pm 8\%$ slower than k_{LNA} (*i.e.* $k_{LNA}' = 0.46 \pm 0.08 \times k_{LNA}$) is needed to account for the kinetic evolution of LNAO and $LNAO_2$ and average number of O atoms per linolenic acid molecule (shown as dashed lines in Fig. S-5 in the ESI†) instead.

4. Conclusions

The heterogeneous reaction of OH radicals, in the presence of H_2O_2 and O_2, with submicron unsaturated fatty acid particles is examined using aerosol mass spectrometry to explore how surface OH addition reactions initiate chain reactions that rapidly transform the chemical composition of an organic particle. The effective uptake coefficients for oleic acid, linoleic acid and linolenic acid are found to be 1.72 ± 0.08, 3.75 ± 0.18 and 5.73 ± 0.14, respectively, in the presence of 20.7 ppm $[H_2O_2]$ at 10% $[O_2]$. Since the effective uptake coefficients of the unsaturated fatty acids are larger than one, this provides clear evidence for particle-phase secondary chain chemistry. The effective uptake coefficient increases linearly with the number of C=C double bonds in the unsaturated fatty acid molecule, indicating that the chain chemistry is initiated by OH addition to the C=C double bond.

Elemental mass spectrometric analysis reveals that functionalization occurs *via* the addition of, on average, 0.57 ± 0.02, 0.61 ± 0.01 and 0.73 ± 0.04 O atoms per reactive loss of oleic acid, linoleic acid and linolenic acid respectively, indicating that OH addition to the C=C double bond is not the sole reaction pathway that consumes the molecular species. This reveals the presence of secondary chain reactions that consume the particle phase molecular species without adding oxygenated functional groups to the particle. Despite the presence of such secondary chain reactions, the oxidative transformation of the unsaturated fatty acid particle's average particle mass and chemical composition is controlled by functionalization reactions at the initial stages of oxidation, with fragmentation reactions being a minor reaction channel. However, volatilization becomes an increasingly important loss channel for particulate organic matter at high OH exposures, where the aerosol contains an increasing fraction of oxygenated functional groups.

The effective uptake coefficients of the unsaturated fatty acid particles are also found to be dependent on $[O_2]$, $[H_2O_2]$ and [OH] in the flow reactor. For each unsaturated fatty acid, the effective uptake coefficient decreases before leveling off when $[O_2]$ in the flow reactor is increased. When $[H_2O_2]$ in the flow reactor is increased, the effective uptake coefficient decreases. In addition, the effective uptake coefficient is found to decrease when the absolute [OH] in the flow reactor is increased. This correlation between the effective uptake coefficient and $[O_2]$ and [OH] arises from the competitive rates of chain propagation and termination reactions. The correlation between the effective uptake coefficient and $[H_2O_2]$ can be attributed to H_2O_2 adsorbing to the particle surface and blocking reaction sites at the particle surface. These results demonstrate that for heterogeneous reactions involving secondary chain chemistry, reaction rates depend sensitively on the concentrations of species that act as radical initiators, chain propagators and terminators in the free radical chain reactions.

Acknowledgements

T. N., S. R. L. and K. R. W. are supported by the Director, Office of Energy Research, Office of Basic Energy Sciences, Chemical Sciences Division of the U.S. Department of Energy under Contract No. DE-AC02-05CH11231. K. R. W. is additionally supported by the Department of Energy, Office of Science Early Career Research Program. J. H. K., S. H. K. and K. E. D. are supported by the National Science Foundation (Grants No. CHE-1012809 and AGS-1056225).

References

1 R. Atkinson, *J. Phys. Chem. Ref. Data*, 1994, Monograph 2, R1–R216.
2 R. Atkinson, *J. Phys. Chem. Ref. Data*, 1997, **26**, 215–290.

3 R. Atkinson and J. Arey, *Chem. Rev.*, 2003, **103**, 4605–4638.
4 A. A. Boyd and R. Lesclaux, *Int. J. Chem. Kinet.*, 1997, **29**, 323–331.
5 A. A. Boyd, R. Lesclaux, M. E. Jenkin and T. J. Wallington, *J. Phys. Chem.*, 1996, **100**, 6594–6603.
6 A. A. Boyd, E. Villenave and R. Lesclaux, *Atmos. Environ.*, 2003, **37**, 2751–2760.
7 C. L. Liu, J. D. Smith, D. L. Che, M. Ahmed, S. R. Leone and K. R. Wilson, *Phys. Chem. Chem. Phys.*, 2011, **13**, 8993–9007.
8 T. Moise and Y. Rudich, *Geophys. Res. Lett.*, 2001, **28**, 4083–4086.
9 D. L. Che, J. D. Smith, S. R. Leone, M. Ahmed and K. R. Wilson, *Phys. Chem. Chem. Phys.*, 2009, **11**, 7885–7895.
10 V. F. McNeill, R. L. N. Yatavelli, J. A. Thornton, C. B. Stipe and O. Landgrebe, *Atmos. Chem. Phys.*, 2008, **8**, 5465–5476.
11 I. J. George and J. P. D. Abbatt, *Nat. Chem.*, 2010, **2**, 713–722.
12 J. H. Kroll, J. D. Smith, D. L. Che, S. H. Kessler, D. R. Worsnop and K. R. Wilson, *Phys. Chem. Chem. Phys.*, 2009, **11**, 8005–8014.
13 J. D. Smith, J. H. Kroll, C. D. Cappa, D. L. Che, C. L. Liu, M. Ahmed, S. R. Leone, D. R. Worsnop and K. R. Wilson, *Atmos. Chem. Phys.*, 2009, **9**, 3209–3222.
14 J. H. Kroll, N. M. Donahue, J. L. Jimenez, S. H. Kessler, M. R. Canagaratna, K. R. Wilson, K. E. Altieri, L. R. Mazzoleni, A. S. Wozniak, H. Bluhm, E. R. Mysak, J. D. Smith, C. E. Kolb and D. R. Worsnop, *Nat. Chem.*, 2011, **3**, 133–139.
15 K. R. Wilson, J. D. Smith, S. H. Kessler and J. H. Kroll, *Phys. Chem. Chem. Phys.*, 2012, **14**, 1468–1479.
16 I. J. George, A. Vlasenko, J. G. Slowik, K. Broekhuizen and J. P. D. Abbatt, *Atmos. Chem. Phys.*, 2007, **7**, 4187–4201.
17 S. H. Kessler, T. Nah, K. E. Daumit, J. D. Smith, S. R. Leone, C. E. Kolb, D. R. Worsnop, K. R. Wilson and J. H. Kroll, *J. Phys. Chem. A*, 2012, **116**, 6358–6365.
18 S. H. Kessler, J. D. Smith, D. L. Che, D. R. Worsnop, K. R. Wilson and J. H. Kroll, *Environ. Sci. Technol.*, 2010, **44**, 7005–7010.
19 J. D. Hearn and G. D. Smith, *Geophys. Res. Lett.*, 2006, **33**, L17805.
20 C. R. Ruehl, T. Nah, G. Isaacman, D. R. Worton, A. W. H. Chan, K. R. Kolesar, C. D. Cappa, A. H. Goldstein and K. R. Wilson, *J. Phys. Chem. A*, 2013, **117**, 3990–4000.
21 T. M. D'andrea, X. Zhang, E. B. Jochnowitz, T. G. Lindeman, C. J. S. M. Simpson, D. E. David, T. J. Curtiss, J. R. Morris and G. B. Ellison, *J. Phys. Chem. B*, 2008, **112**, 535–544.
22 S. G. Moussa and B. J. Finlayson-Pitts, *Phys. Chem. Chem. Phys.*, 2010, **12**, 9419–9428.
23 M. C. Ball and S. Massey, *Thermochim. Acta*, 1995, **261**, 95–106.
24 B. Warscheid and T. Hoffmann, *Rapid Commun. Mass Spectrom.*, 2002, **16**, 496–504.
25 A. C. Aiken, P. F. DeCarlo and J. L. Jimenez, *Anal. Chem.*, 2007, **79**, 8350–8358.
26 A. C. Aiken, P. F. Decarlo, J. H. Kroll, D. R. Worsnop, J. A. Huffman, K. S. Docherty, I. M. Ulbrich, C. Mohr, J. R. Kimmel, D. Sueper, Y. Sun, Q. Zhang, A. Trimborn, M. Northway, P. J. Ziemann, M. R. Canagaratna, T. B. Onasch, M. R. Alfarra, A. S. H. Prevot, J. Dommen, J. Duplissy, A. Metzger, U. Baltensperger and J. L. Jimenez, *Environ. Sci. Technol.*, 2008, **42**, 4478–4485.
27 P. F. DeCarlo, J. R. Kimmel, A. Trimborn, M. J. Northway, J. T. Jayne, A. C. Aiken, M. Gonin, K. Fuhrer, T. Horvath, K. S. Docherty, D. R. Worsnop and J. L. Jimenez, *Anal. Chem.*, 2006, **78**, 8281–8289.
28 J. T. Jayne, D. C. Leard, X. F. Zhang, P. Davidovits, K. A. Smith, C. E. Kolb and D. R. Worsnop, *Aerosol Sci. Technol.*, 2000, **33**, 49–70.
29 R. Atkinson, *Atmos. Chem. Phys.*, 2003, **3**, 2233–2307.
30 Y. Rudich, N. M. Donahue and T. F. Mentel, *Annu. Rev. Phys. Chem.*, 2007, **58**, 321–352.
31 K. S. Docherty and P. J. Ziemann, *J. Phys. Chem. A*, 2006, **110**, 3567–3577.
32 T. Hoffmann, R. Bandur, S. Hoffmann and B. Warscheid, *Spectrochim. Acta, Part B*, 2002, **57**, 1635–1647.
33 L. Lee, P. Wooldridge, T. Nah, K. Wilson and R. Cohen, *Phys. Chem. Chem. Phys.*, 2013, **15**, 882–892.
34 Z. J. Zhao, S. Husainy, C. T. Stoudemayer and G. D. Smith, *Phys. Chem. Chem. Phys.*, 2011, **13**, 17809–17817.
35 J. W. Morris, PhD thesis, Boston College, Chestnut Hill, Massachusetts, 2002.
36 J. D. Hearn, A. J. Lovett and G. D. Smith, *Phys. Chem. Chem. Phys.*, 2005, **7**, 501–511.
37 M. Iwahashi, Y. Kasahara, H. Matsuzawa, K. Yagi, K. Nomura, H. Terauchi, Y. Ozaki and M. Suzuki, *J. Phys. Chem. B*, 2000, **104**, 6186–6194.
38 P. F. DeCarlo, J. G. Slowik, D. R. Worsnop, P. Davidovits and J. L. Jimenez, *Aerosol Sci. Technol.*, 2004, **38**, 1185–1205.
39 S. V. Vasenkov, V. A. Bagryansky, V. V. Korolev and V. A. Tolkatchev, *Radiat. Phys. Chem.*, 1991, **38**, 191–197.
40 G. Odian, *Principles of Polymerization*, John Wiley & Sons, Inc., New Jersey, 2004.
41 Y. K. Bhardwaj, H. Mohan, S. Sabharwal and A. B. Majali, *Radiat. Phys. Chem.*, 2000, **58**, 373–385.
42 V. Kumar, Y. K. Bhardwaj, S. Sabharwal and H. Mohan, *J. Radiat. Res.*, 2003, **44**, 161–169.
43 L. H. Renbaum and G. D. Smith, *Atmos. Chem. Phys.*, 2011, **11**, 6881–6893.
44 J. H. Slade and D. A. Knopf, *Phys. Chem. Chem. Phys.*, 2013, **15**, 5898–5915.
45 K. U. Ingold, *Acc. Chem. Res.*, 1969, **2**, 1–2.
46 C. von Sonntag and H. P. Schuchmann, *Angew. Chem., Int. Ed. Engl.*, 1991, **30**, 1229–1253.
47 C. von Sonntag, P. Dowideit, X. W. Fang, R. Mertens, X. M. Pan, M. N. Schuchmann and H. P. Schuchmann, *Water Sci. Technol.*, 1997, **35**, 9–15.
48 J. D. Hearn, L. H. Renbaum, X. Wang and G. D. Smith, *Phys. Chem. Chem. Phys.*, 2007, **9**, 4803–4813.
49 E. S. C. Kwok and R. Atkinson, *Atmos. Environ.*, 1995, **29**, 1685–1695.